Solid Freeform Fabrication 2019: Proceedings of the 30th Annual International Solid Freeform Fabrication Symposium – An Additive Manufacturing Conference
Reviewed Paper

Evaluating the corrosion performance of wrought and additively manufactured (AM) Invar ® and 17-4PH

I.S. Grech*, Dr N.Wint*, Dr S. Mehraban*, Prof. J. Sullivan* and Prof. N. Lavery*

*Department of materials science, Swansea University, Wales, SA1 8EN

Abstract

A Renishaw AM 400 was used to produce Laser Powder Bed fusion (LPBF) iron alloy Invar ® and 17-4PH components. Build parameters were systematically changed and the corrosion performance of the samples produced was investigated using a combination of scanning vibrating electrode technique (SVET) and advanced conventional electrochemical techniques. The results indicated that small changes in the density of the LPBF parts due to porosity resulted in large changes to the materials corrosion susceptibility. The LPBF samples also demonstrated significantly more variation in pitting potential measurements compared to wrought samples indicating inhomogeneity in the built parts. References to AM samples in this work refer to samples produced using LPBF.

Introduction

LPBF is a new and complex technique that prints metallic parts directly from CAD files. This technique has a great number of variables to consider including laser, geometrical and build chamber variables. While there is limited information available regarding the effect of varying build parameters on the mechanical properties of printed components [1]; the way these variables impact the corrosion performance of LPBF parts is largely unknown. This lack of knowledge regarding the reliability and reproducibility of parts limits the integration of AM into several industries, particularly those in which safety critical components are used. This work aims to identify the differences in the corrosion performance of LPBF and wrought parts and understand the reasons behind these differences.

The freedom of design that AM offers is of significant interest to industry including the Defence Support Services sector [2]. The development and increased understanding of AM processes would allow for bespoke parts to be produced as and when required, reducing both the storage space required and the costs of shipping individual components. Consideration must be given to the operating environment and the needs for resistance to shock, vibrations, controlled atmospheres, as well as corrosion, particularly in maritime environments, where components are subject to harsh conditions. The high cooling rates associated with LPBF could result in different phase ratios, while unmelted powder can result in porous components. Additionally, the effects of anisotropic and heterogeneous microstructure must be understood for AM to be incorporated in industry.

The flexibility of LPBF means that a range of materials can be printed including single and multi-phase alloys. The materials studied in this work were selected with the aim of obtaining as much information regarding the corrosion performance of AM components as possible. To this end, Invar ®, a low thermal expansion alloy comprising of 27% Ni and bal. Fe, was selected alongside 17-4PH stainless steel which has sufficient chromium content to form a passive oxide layer. 17-4 PH stainless steel is vulnerable to pitting corrosion which occurs due to localised breakdown of its passive oxide layer. Passive oxide layers form naturally on some materials surfaces. These layers are usually a few nanometres thick and greatly reduce the rate of corrosion of the metal in the presence of aggressive anions [3]. Localised breakdown of the passive oxide layer can result in the initiation of pitting corrosion. Active pits can perforate the structure of the material and can act as initiation sites for cracks leading to a reduction in the structural integrity of components [4].

During this work LPBF was used to produce iron alloy Invar ® and 17-4PH components. Build parameters are systematically changed and the corrosion performance of the samples produced is investigated using a combination of scanning vibrating electrode technique (SVET) and advanced conventional electrochemical techniques.

Experimental Methods

LPBF Parameter Optimisation and Sample Preparation

17-4PH and Invar ® cubes with side lengths of 15 mm were printed using a Renishaw AM 400 LPBF system. The build parameters for these cubes were chosen based on an iterative process whereby component density was optimised [5]. Samples were then polished to a 1 μm finish and subject to a range of corrosion tests including SVET and polarisation. For each powder used, build parameters must be optimised to produce high density components with mechanical properties comparable to their wrought counterparts. Information gained from printing in powder of similar elemental composition and geometry can be used as a starting point for this process. The volumetric Energy Density (VED) equation is displayed in equation 1,

$$VED = \frac{P \cdot ET}{PD \cdot HS \cdot LT} \quad (1)$$

where P is power, ET is the laser exposure time, PD is the point distance, HS is the hatch spacing and LT is the layer thickness. The VED conveys the quantum of energy which is deposited within each sample during the powder melting process. Orthogonal arrays were created to produce components with variable energy densities an example of which is displayed in table 1. Several repeat arrays were constructed across the build plate to account for any variation in build quality which could arise due to inhomogeneous gas flow or other

geometrical factors. Density measurements were carried out on 15 mm^3 density cubes using an Attention Sigma 700 force tensiometer which measures the change in force recorded as the sample is immersed in deionised water. The software then uses Archimedes principle to calculate the density of each sample. Statistical analysis was then carried out on the data which fed into the iterative process for the optimisation of build parameters. Cubes, optimised for density, were then selected for corrosion testing. Cubes were sectioned such that several samples were attained from each cube whilst removing the cubes outer finish. All samples were ground and polished to a 1 µm finish to ensure that any differences in corrosion performance was as a result of the variation of build parameters as opposed to varying surface roughnesses.

Table 1- 17-4 PH orthogonnal aray build parameters

Sample Label	Point distance (µm)	Hatch Spacing (µm)	Exposure time (ms)	Power (W)	Energy Density (J/mm^3)
1	60	60	60	180	60
2	60	80	90	215	81
3	60	100	120	250	100
4	80	60	90	250	94
5	80	80	120	180	67
6	80	100	60	215	32
7	100	60	120	215	86
8	100	80	60	250	38
9	100	100	90	180	32

Potentiodynamic polarisation

Potentiodynamic polarisation allows for information on the corrosion rate, pitting susceptibility and passivity of an electrochemical system to be determined [6]. When performing a DC polarisation scan, the ionic conduction path is provided through the solution separating the working and counter electrodes, while the electrical conduction path is provided through a potentiostat which controls the voltage difference between the working and reference electrode [6]. The potentiodynamic measurements made in this work were carried out using a custom-made plastic sample holder which allowed an electrical connection to be made to the underside of the sample whilst isolated from the electrolyte. This would allow the polished surface of the sample to be immersed and function as the working electrode in this setup. In an

anodic polarization scan the potential is driven in the anodic direction, causing the sample/working electrode to become anodic whilst electrons flow from the sample through the circuit to the counter electrode. In this work the recorded current density represents the rate at which the anodic reactions are taking place on the sample/working. This type of scanning is appropriate for investigating materials which readily form a passive oxide film such as stainless steels. Cyclic potentiodynamic polarization is a method of potentiodynamic scanning wherein the applied potential is reversed at the highest applied voltage and reduced to below the open circuit potential (OCP). The reverse section of the scan is used to investigate a materials ability to repassivate. Voltages are quoted relative to the saturated calomel electrode (SCE) and a conventional platinum counter electrode was used with the Solatron 1280 potentiostat galvonostat in the standard three cell setup [6]. The scanning direction was reversed in this work when a current density of 0.5 Acm^{-2} was recorded.

Potentiodynamic scanning was used in this work to explore the pitting and repassivation behaviour of a range of 17-4 PH AM samples with a range of energy densities for comparison with wrought 17-4PH samples. The scans were programmed to record the OCP of the samples for 10 minutes before beginning an anodic sweep starting 200 mV below the OCP and continuing to 1.5V. This scanning range was sufficient to polarise the samples to the point of pitting corrosion and complete sample breakdown. Visual inspection of all samples during and post scanning confirmed that pitting corrosion had taken place.

SVET

For SVET measurements, samples were polished before being immersed in a 0.17M NaCl electrolytic solution. The SVET microtip probe scans in a raster fashion 150 μm from the surface of the sample scanning. The SVET was configured to record data every 0.2 mm, with a dwell time of 50 ms allowing for 5 measurements per point with a probe oscillation frequency of 140 Hz raster scanning across the sample once every hour for 24 hours. This allows the SVET to collect spatial and temporal mechanistic information over a defined area for a set period of time [7]. The SVET registers an alternating potential that is proportional to the electric field strength in the vertical direction. This alternating potential is produced from the oscillation of the SVET tip in the potential field which is generated by the ionic current flux that passes through the electrolyte solution. This point scan data is then stitched together to produce a sample map at each time step with anodic and cathodic regions visible [7]. SVET scanning was used in this work to observe the difference in the corrosion rate between wrought and AM Invar ® while immersed in ambiently aerated 0.17M NaCl electrolyte. Further manipulation of SVET data allows for the mass loss and mass loss rate due to corrosion to be calculated by making use of the Faraday law and assuming that the corrosion activity occurring on the sample remains constant in the interval between scans. A detailed explanation of the mathematical process is provided elsewhere [8].

Results and discussion

Material Density Profiles

Figures 1 and 2 show the measured density as a function of volumetric energy density of Invar ® and 17-4PH respectively. The plotted values represent average values from multiple repeat readings with the standard deviation of these readings being used for the error bars. The curves obtained are a similar shape for both materials and the relationship between density and volumetric energy density is independent of build material. At low energy densities incomplete powder melting results in low measured densities. The curves then plateau and tend towards the natural maximum density value for each material. In Figure 2 the measured density of the samples begins to drop off after ~100 J/mm^3. This may be caused by the vapourisation of powder at high energy levels which reduces the homogeneity of melted powder and results in keyholing and build defects [9]. The range of energy density values selected were centred on the maximum density values shown in Figure 1 and Figure 2. Components for corrosion testing were constructed between VED's of 43.25 – 60.00 J/mm^3 for Invar ® and 32.25 - 100.00 J/mm^3 for 17-4PH.

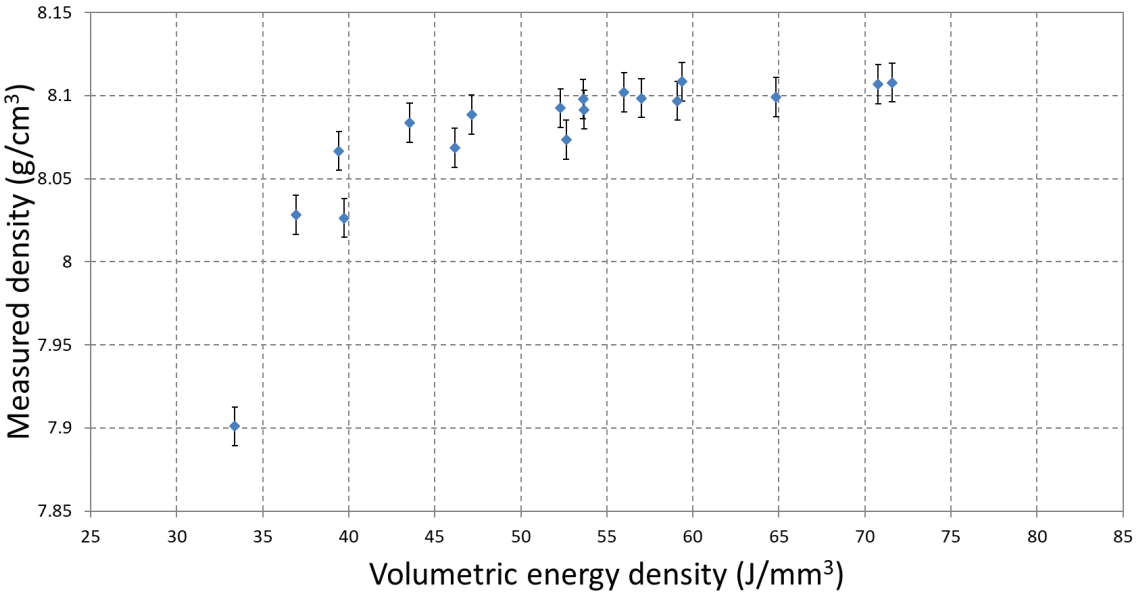

Figure 1- Invar ® material density profile

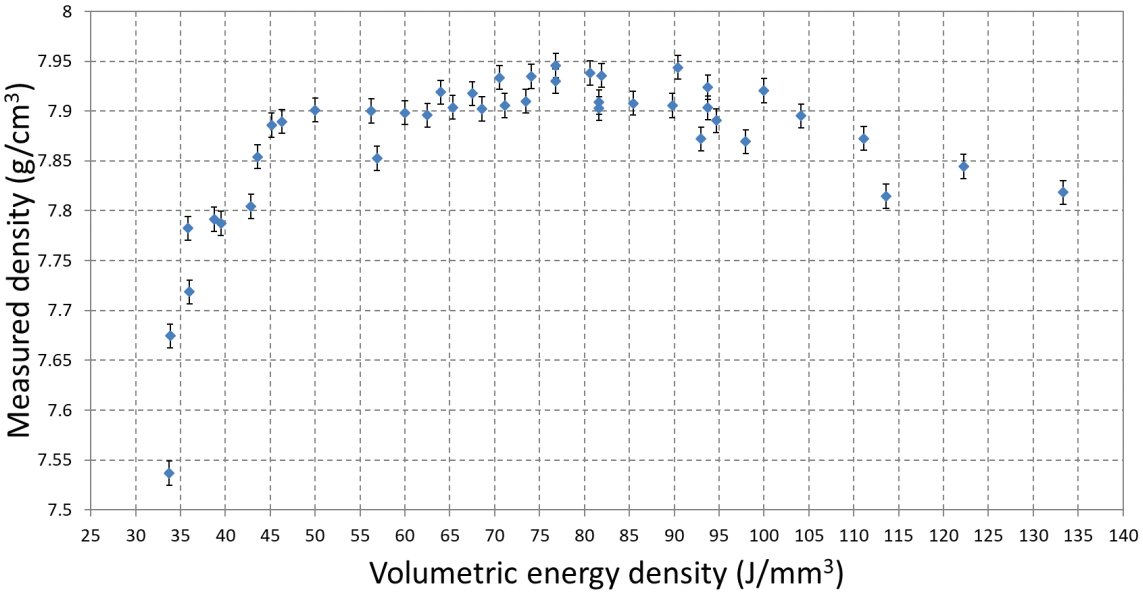

Figure 2- 17-4 PH material density profile

Invar ® – SVET

A range of wrought and AM samples immersed in 0.17M NaCl solution were scanned using SVET. In all cases, the mass lost from wrought samples was less than the mass lost from the AM samples. After 20 hours of SVET scanning the AM samples lost on average 0.3097 ± 0.1606 g.cm^{-2} of material compared to the wrought value of 0.0032 ± 0.0180 g.cm^{-2}. Figure 3 shows SVET derived false colour maps from scans of a wrought and an AM sample built with a VED of 59.36 J/mm^3 and a measured density of (100.1 ± 0.2) % relative to wrought invar.

The red regions in the SVET false colour maps represent anodic areas where corrosion has initiated. The difference between the wrought and AM sample is clearly visible with the AM sample displaying several anodic regions forming after 5 hours. Subsequently these anodic regions increase in intensity over time in the top left anodic region from 1.0 A.m^{-2} after 5 hours to 6.0 A.m^{-2} after 29 hours. The wrought sample does not display any form of anodic attack within the first 5 hours. After 29 hours there is some low intensity anodic activity along the left boundary of the sample represented by the white region. This low activity does not represent significant corrosion attack. The different scale bars on the wrought and AM sample SVET false colour maps reinforce the difference in anodic activity with the highest level of anodic activity in the wrought sample after 29 hours measuring a current density of 0.3 A.m^{-2}. Visual examination of the samples post immersion confirms the absence of corrosion product on the wrought sample. The corrosion that occurred to the AM sample focussed around the anodic areas as displayed in the optical images in figure 3. It is possible that build defects on the invar

sample surface allow aggressive halide species to migrate into the sample and corrode the inside of the sample.

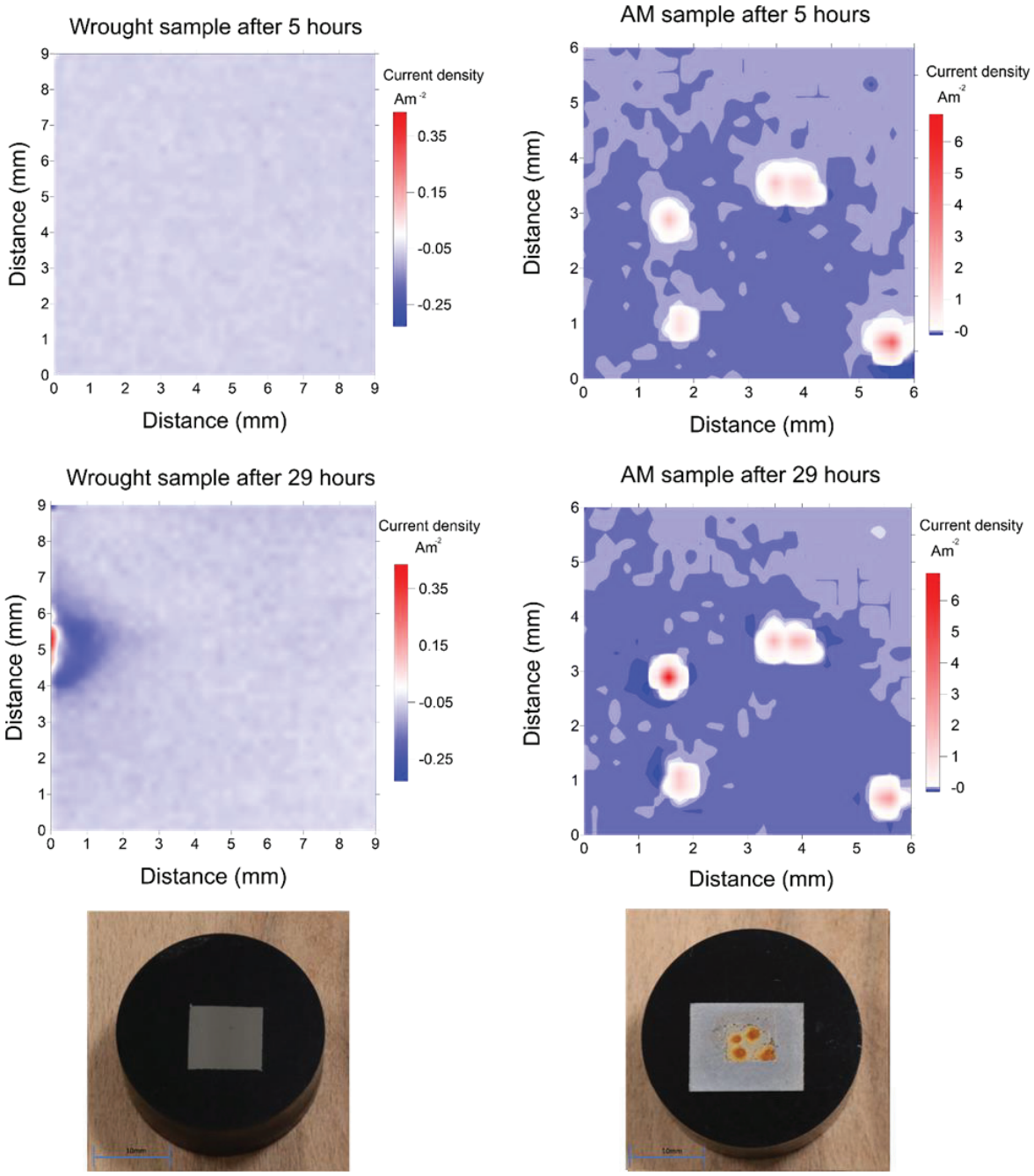

Figure 3- SVET derived false colour maps of wrought AM invar with optical images showing samples post corrosion testing

Potentiodynamic Scanning

Table 2 displays the mean pitting potentials for tested samples as well as their measured density. Sample 6, the lowest density sample demonstrates the lowest pitting potential. The fact that the value is negative is not significant as the values are quoted relative to SCE in this case. The data shows that sample 3, the AM sample with the highest density outperformed every other tested sample with the highest measured average pitting potential. However, this sample also exhibited the largest variation in pitting potentials. Further to this the variation of pitting potentials recorded indicates that the wrought samples demonstrate better repeatability than the AM samples. The average variability recorded for the wrought samples are 7% compared to 80% for the AM samples. The larger spread of pitting potentials recorded in repeat measurements of AM samples could be due to sample inhomogeneity with regards to the random location of build defects. Any build defect on, or near, the surface in a sample could result in a reduction in the uniformity of the samples passive oxide layer reducing its effectiveness.

It is also apparent that a small decrease in the density of AM parts results in a significant reduction in the pitting potential. This could be indicative of samples with densities below a certain threshold being more vulnerable to pitting due to there being more build defects acting as initiation sites for pitting on the surface of the sample. The difference between the wrought and unpolished values justifies the reasoning behind polishing all samples and discounting surface roughness effects as the polished wrought samples have significantly higher pitting potentials than their unpolished wrought counterparts.

Table 2 - Average pitting potential values for AM and wrought 17-4PH samples

Sample	Density (%)	Average Pitting Potential (V) vs SCE
1	99.46 ± 0.01	0.051 ± 0.031
3	99.78 ± 0.01	0.332 ± 0.283
4	99.56 ± 0.01	0.023 ± 0.017
6	93.67 ± 0.01	-0.192 ± 0.190
Wrought	-	0.293 ± 0.009
Unpolished Wrought	-	0.176 ± 0.021

The polarisation curves displayed in Figure 4 convey the difference between the samples with the highest and lowest pitting potentials, samples 3 and 6 respectively. The regions labelled A and B represent the passive region of each sample respectively. The passive region of sample 6 is severely diminished compared to the passive region in sample 3. A decreased passive region has been reported previously in literature for AM parts with the

observation being attributed to elemental segregation, retained oxides, and/or porosity [10]. Additionally, the sharp horizontal extensions from the sample 3's passive region are indicative of metastable pitting where pits are initiated and re-passivated quickly before they can mature in stable pits [11]. The open circuit potential (OCP) is the potential at which the sum of the anodic and cathodic reaction rates on the electrode surface is zero. The more negative OCP value of sample 6 is also indicative of a system more thermodynamically susceptible to anodic attack compared to sample 3.

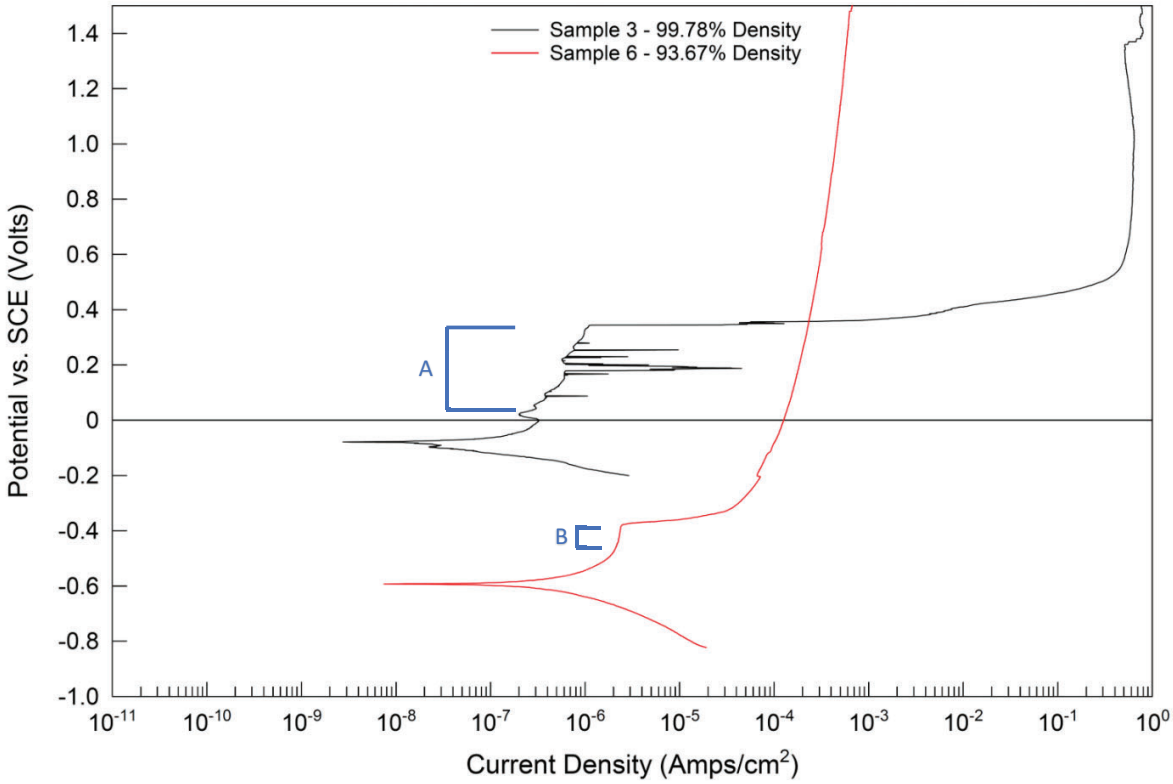

Figure 4 – Anodic polarisation scans for AM samples immersed in 0.6M NaCl electrolyte.

Figure 5 displays cyclic potentiodynamic polarization loops for AM sample 3 and a wrought sample. The nature of the hysteresis loop of a potentiodynamic scan yields information regarding corrosion performance within the electrolyte. For example, a negative hysteresis loop with a passivation potential well above the OCP indicates that the testing material will not readily corrode while in service in conditions representative of the electrolyte used [12]. The cyclic potentiodynamic polarization loops in figure 5 show that the AM samples passive oxide layer broke down at a higher potential than the wrought sample which is in agreement with the data in Table 2. Although both scans demonstrate a positive hysteresis loop, the wrought sample demonstrates repassivation at the area labelled Repass. (where the reverse direction negative scan intersects the initial positive anodic scan).

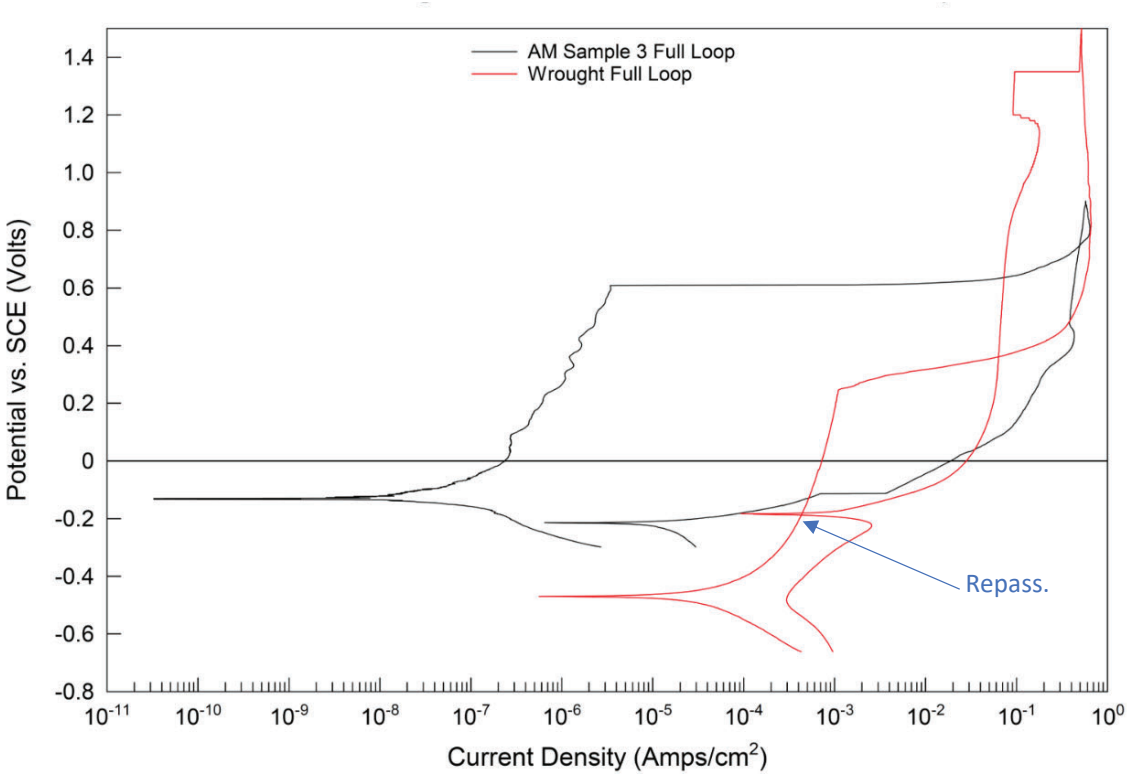

Figure 5- Cyclic potentiodynamic polarization loops for wrought and AM sample 3

The repassivation potential is ~0.28 V higher than the OCP. This large difference is the result of disruption of the passive oxide layer at high potentials, with the large hysteresis loop suggesting significant passive film disruption indicating that the material immersed in this solution would be susceptible to pitting over time while in service in the same environment [11].

Repassivation of the AM samples is not observed (the cathodic direction scan does not intersect the initial anodic scan) and the hysteresis loop is open. The summary of this data is that the AM sample with the highest pitting potential demonstrates a greater resistance to pitting initially than the wrought sample. However, once pitting has begun and the passive oxide film has been broken down the wrought sample is able to repair its passive oxide layer and repassivate active pits whereas the AM sample cannot and active pits continue to degrade the sample. This is further demonstrated by much higher current density in the reverse direction of the CPP scans for the AM sample compared to wrought. The reason behind this is not clear and further investigation is needed to understand this.

Conclusions and Further Work

The corrosion performance of wrought and AM Invar ® was compared using SVET. The SVET data showed that anodic regions were formed on the AM sample after immersion for 5 hours whereas the wrought sample showed very little anodic activity. The increased mass loss exhibited by the AM samples compared to the wrought samples demonstrates the reduced performance of AM Invar ® in the marine environment. Further work to investigate Invar ® could include using a micro indenter to create porosity in a wrought Invar ® sample. This would allow for differentiating reduced corrosion resistance due to porosity or other effects from the LPBF process.

The pitting corrosion performance of AM and wrought 17-4PH was investigated using potentiodynamic techniques. The potentiodynamic results indicate that the pitting potential for AM samples varies significantly with small changes in sample density. Whilst the AM sample with the highest measured density, sample 3 demonstrated a higher pitting potential than the wrought samples every other AM sample tested demonstrated a lower pitting potential than their wrought counterparts. This difference was attributed to inhomogeneities in the AM samples. Despite the increased pitting potential of sample 3 the sample was unable to repassivate. Further work regarding 17-4PH could involve exploring various post build heat treatments in an attempt to reduce the porosity and the non-homogeneity of the AM samples.

Acknowledgments

The author would like to thank DSTL for funding this research, the MACH1 centre at Swansea university for the use of their facilities and equipment and Dr Natalie Wint, Dr Shahin Mehraban, Professor James Sullivan and Professor Nicholas Lavery for their support and guidance when carrying out this work.

References

[1] N. Lavery, J. Cherry, A. Davies, H. M. Davies, S. Browgn and J. Sienz, "Investigation into the effect of process parameters on microstructural and physical properties of 316L stainless steel parts by selective laser melting.," *The International Journal of Advanced Manufacturing Technology,* vol. 76, pp. 869-879, 2015.

[2] A. Busachi, "Defining Next-Generation Additive Manufacturing Applications for the Ministry of Defence (MoD)," *Procedia CIRP,* vol. 55, pp. 302-307, 2016.

[3] G. Frankel, "Pitting corrosion of metals a review of the critical factors," *Journal of the electrochemical society,* vol. 145, no. 6, pp. 2186-2198, 1998.

[4] G. T. L. S. J. Frankel, "Perspective—Localized Corrosion: Passive Film Breakdown vs Pit Growth Stability," *Journal of the Electrochemical Socity,* vol. 164, no. 4, pp. 180-181, 2017.

[5] N. Lavery, J. Cherry, S. Mehmood, H. Davies, B. Girling, E. Sackett, S. G. Brown and J. Sienz, "Effects of hot isostatic pressing on the elastic modulus and tensile properties of 316L parts made by powder bed laser fusion," *Material Science and Engineering,* vol. 693, pp. 186-213, 2017.

[6] D. G. Enos, "The potentiodynamic polarization scan: Technical Report 33," University of Virginia, 1997.

[7] D. Worsley and H. Mcmurray, "Scanning electrochemical techniques for the study of localised metallic corrosion," Swansea University, 1997.

[8] J. Sullivan, C. Weirman, J. Kennedy and D. Penney, "Influence of steel gauge on the microstructure and corrosion performance of zinc allow coated steels," *Corrosion Science,* vol. 52, pp. 1853-1862, 2010.

[9] A. Philo, S. Mehraban, S. Sillars, C. J. Sutcliffe, J. Sienz, S. G. Brown and N. Lavery, "A pragmatic continuum level model for the prediction of the onset," *The International Journal of Advanced Manufacturing Technology,* pp. 697-714, 2019.

[10] J. M. T. J. Rebecca F. Schaller, "Corrosion Properties of Powder Bef Fusion Additively Manufactured 17-4 PH Stainless Steel," *Corrosion ,* vol. 73, no. 7, pp. 796-807, 2017.

[11] M. A. H. S. S. Esmailzadeha, "Interpretation of Cyclic Potentiodynamic Polarization Test Results for Study of Corrosion Behaviour of Metals: A Review," *Protection of Metals and Physical Chemistry of Surfaces,* vol. 54, no. 5, pp. 976-989, 2018.

[12] G. Frankel and J. Beavers, "Recommended protocol for cyclic potentiodynamic polarization curves and data analysis," Ohio State University.